JACS Au
AN OPEN ACCESS JOURNAL OF THE AMERICAN CHEMICAL SOCIETY



pubs.acs.org/jacsau
Article

# Photoexcitation-Assisted Molecular Doping for High-Performance Polymeric Thermoelectric Materials

*Published as part of JACS Au special issue "Polymers for the Clean Energy Transition".*

Zhen Ji, Zhiyi Li, Xiaojuan Dai, Lanyi Xiang, Yue Zhao, Dongyang Wang, Xiao Zhang, Liyao Liu, Zhiyuan Han, Lixin Niu, Yuqiu Di, Ye Zou,* Chong-an Di,* and Daoben Zhu

Cite This: JACS Au 2024, 4, 3884−3895

Read Online

ACCESS | Metrics & More | Article Recommendations | Supporting Information

**ABSTRACT:** Molecular doping plays a crucial role in modulating the performance of polymeric semiconductor (PSC) materials and devices. Despite the development of numerous molecular dopants and doping methods over the past few decades, achieving highly efficient doping of PSCs remains challenging, primarily because of the inadequate matching of frontier energy levels between the host polymers and the dopants, which is critical for facilitating charge transfer. In this work, we introduce a novel doping method termed photoexcitation-assisted molecular doping (PE-MD), capable of transcending limitations imposed by energy level disparities through the mediation of efficient photoinduced electron transfer between polymers and dopants. This approach significantly amplifies the electrical conductivity of the PDPP4T polymer, increasing it by more than 4 orders of magnitude to a maximum value of 349.67 S $cm^{-1}$. Given that only the irradiated region experiences a substantial increase in doping level, the PE-MD process facilitates the photoresist-free and precise patterning of doped polymers at a resolution down to 1 $\mu$m. Furthermore, the enhanced electrical conductivity of the photoexcitation-assisted molecularly doped PDPP4T film promotes efficient thermoelectric conversion, yielding an impressive initial power factor of 226.1 $\mu W\ m^{-1}\ K^{-2}$ and a figure-of-merit ($ZT$) of 0.18, accompanied by improved thermal and ambient stability. The PE-MD strategy not only remarkably elevates the doping level of PSCs toward efficient thermoelectric conversion but also preserves the easy processability of flexible and integrated devices.

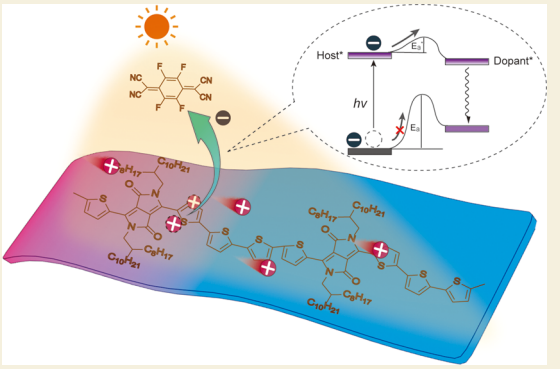


**KEYWORDS:** *polymeric semiconductor, molecular doping, patterned doping, photoexcitation, organic thermoelectric materials*

## 1. INTRODUCTION

Doping is essential for adjusting the electrical properties of polymeric semiconductors (PSCs), i.e., enhancing their performance in a variety of applications, including thermoelectric (TE) materials,[1,2] solar cells,[3,4] and field-effect transistors (FETs).[5,6] Molecular doping of $\pi$-conjugated polymers entails intermolecular charge transfer between the host polymers and the dopants in the ground state.[7−10] Taking p-type doping as an example, efficient p-doping usually requires that the lowest unoccupied molecular orbital (LUMO) energy level of dopants is ideally equal to or deeper than the highest occupied molecular orbital (HOMO) energy level of the host polymers.[11−13] With this in mind, various molecular dopants with deep LUMO levels, such as F4TCNQ,[14] CN6-CP,[15] and Mo(tfd-COCF3),[16] have been engineered to facilitate efficient p-doping of PSCs. However, deepening the LUMO level (or electron affinity) of p-dopants often leads to chemical instability, adversely affecting the long-term stability of the devices.[17,18]

Donor−acceptor (D−A) conjugated copolymers, characterized by alternating sequences of donor (electron-rich) and acceptor (electron-deficient) units, have been demonstrated with vital applications in organic electronics, e.g., causing breakthroughs in FET mobility[19,20] and TE figure-of-merit ($ZT$)[21−24] of PSCs. However, the D−A structure is supposed to be difficult to achieve a high doping level by molecular dopants owing to the acceptor (donor) moiety being inactive for p-type (n-type) doping,[25] making efficient doping of D−A polymers remain a significant challenge. For instance, the typical number of free charges per dopant is only approximately 0.04 in a D−A copolymer by a molecular dopant.[26,27] Only a few dopants with a strong oxidation

Received: June 30, 2024
Revised: August 4, 2024
Accepted: August 9, 2024
Published: August 15, 2024

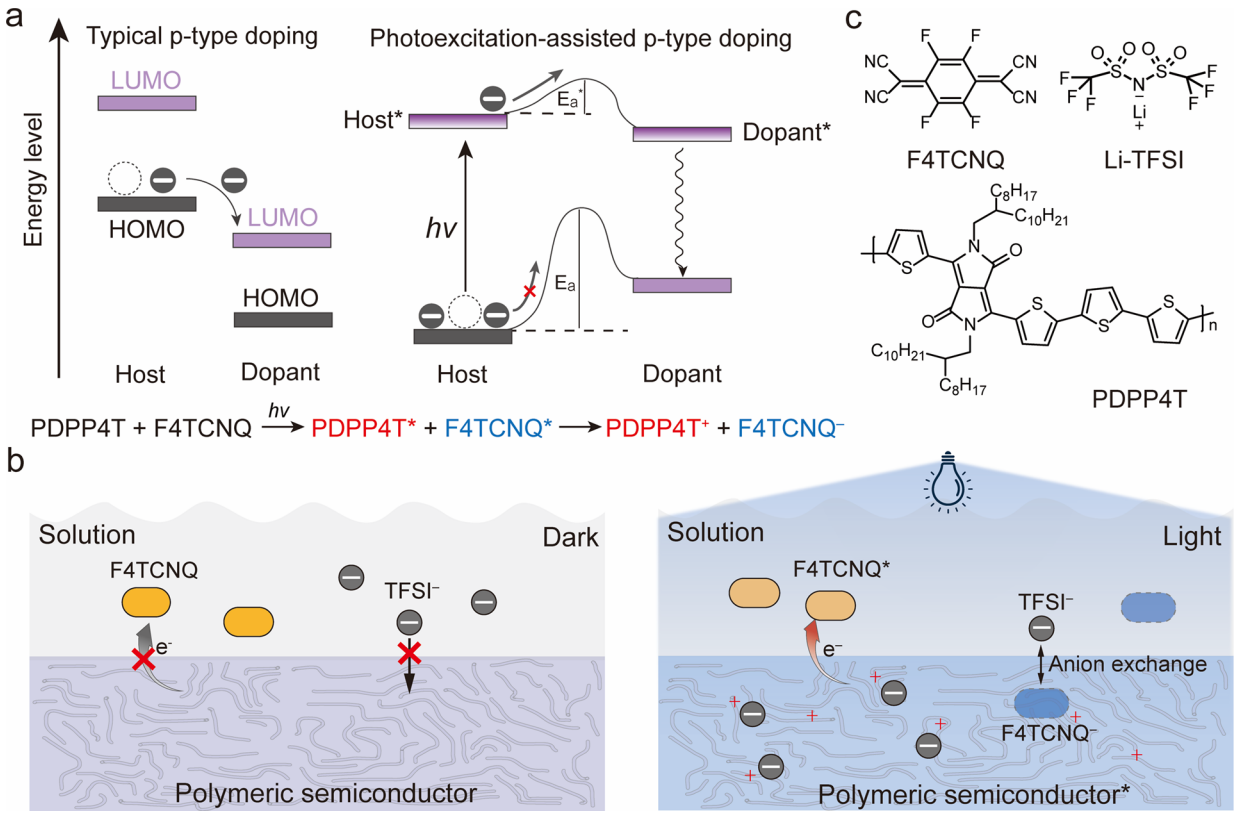


**Figure 1.** PE-MD concept. (a) Principle and (b) schematic diagrams of the molecular p-type doping process for conventional typical doping (left) and PE-MD (right). (c) Chemical structures of the PDPP4T polymer, F4TCNQ dopant, and Li-TFSI salt.

potential such as $FeCl_3$ have demonstrated high doping efficiency for D−A copolymers.[21,22,28] However, achieving high state-of-the-art TE performance necessitates a comprehensive consideration that extends beyond oxidizing properties, such as the size, polarity, and stability of dopants.[1,29,30] The demand calls for the development of new highly efficient dopants or the exploration of innovative doping methods. In this vein, recent promising attempts such as anion-exchange doping,[12,31] transition-metal-catalyzed molecular doping,[32] and photocatalysis doping[33] were proposed to substantially increase the doping level of polymers or even D−A copolymers.

In this work, we present a new strategy based on the well-known process of photoinduced electron transfer (P-ET)[34] to overcome the limitation of insufficient charge transfer between host polymers and dopants employing photoexcitation-assisted molecular doping (PE-MD) without using photocatalysts (Figure 1). We focused on the molecular doping of a typical D−A polymer poly[2,5-bis(2-octyldodecyl)pyrrolo[3,4-*c*]-pyrrole-1,4(2*H*,5*H*)-dione3,6-diyl-*alt*(22,2′;5′,2″;5″,2‴quater-thio-phen-5,5‴-diyl)] (PDPP4T) and a representative dopant 2,3,5,6-tetrafluoro-7,7,8,8-tetracyanoquinodimethane (F4TCNQ), as depicted in Figure 1c. The ionic liquid salt bis(trifluoromethane)sulfonimide lithium (Li-TFSI) was utilized as a counterion to further augment the doping level.[31] We demonstrated the efficacy of PE-MD for precise patterned doping, achieving a 1 $\mu$m photolithographic resolution with a lateral extended doping length of less than 100 nm without using a photoresist. This technique was seamlessly integrated into the fabrication of the polymer FET, where PDPP4T doped via the PE-MD method acted effectively as the source and drain electrodes. Through PE-MD, the electrical conductivity ($\sigma$) of PDPP4T exceeded that achieved through ground-state doping by over 4 orders of magnitude. This advancement enabled a maximum power factor (PF) and *ZT* of up to 226.1 $\mu$W m$^{-1}$ K$^{-2}$ and 0.18, respectively. The results pave the way for both the heightened doping level and photoresist-free patterned doping of D−A polymers, propelling forward an effective approach for the development of high-performance polymeric TE materials and easy-to-process flexible integrated devices.

## 2. RESULTS AND DISCUSSION

### 2.1. PE-MD of PSCs

The PE-MD concept is illustrated in Figure 1. In conventional typical p-type doping, owing to the matched energy levels, electrons are spontaneously injected from the HOMO of the host polymer to the LUMO of the dopant in the ground state. This process results in the formation of holes within the polymer, thus achieving p-doping (left panel in Figure 1a). However, for weak dopants, efficient charge transfer in the ground state is challenging and requires a large thermal activation energy ($E_a$), which thereby often restricts the doping level.[35,36] In contrast, PE-MD leverages photoexcitation to promote an electron from the ground state to a higher excited state (denoted as a host*), generating a vacancy in the ground-state molecular orbital, as illustrated in the right panel of Figure 1a. The promoted electron in this excited state can then be more easily transferred to the dopant or an already excited dopant (dopant*) with a markedly reduced activation energy ($E_a$*). As a result, PE-MD tremendously increases the charge transfer probability via P-ET, enabling a substantially enhanced doping level of the host polymer.


https://doi.org/10.1021/jacsau.4c00567
JACS Au 2024, 4, 3884−3895

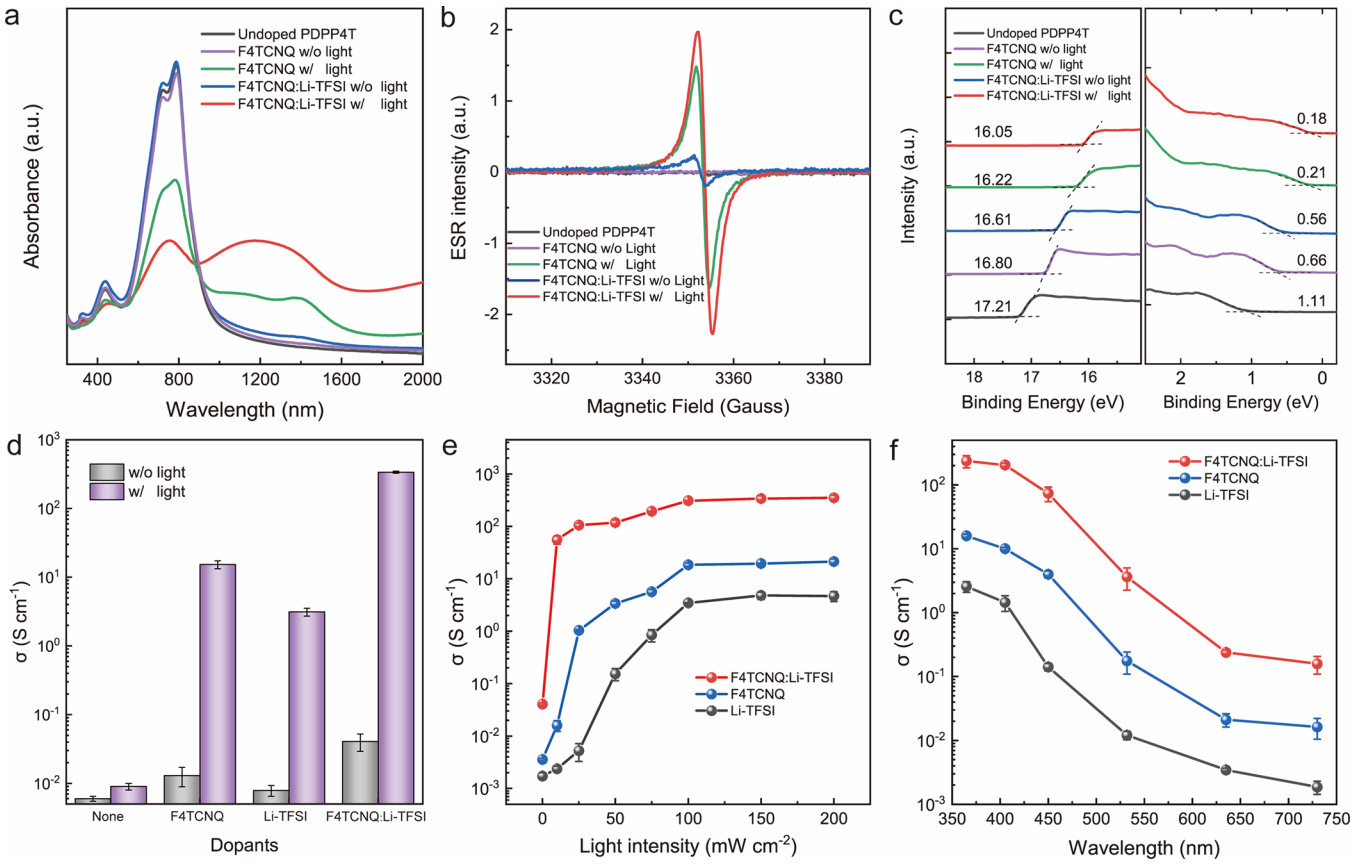


**Figure 2.** Characterization of PE-MD of PDPP4T films. (a) UV−vis−NIR absorption spectra, (b) ESR spectra, and (c) UPS spectra of PDPP4T films doped by F4TCNQ or F4TCNQ:Li-TFSI with (w/) or without (w/o) photoexcitation (white light, 100 mW $cm^{-2}$, 20 min). (d) Electrical conductivity of PDPP4T films doped by F4TCNQ, Li-TFSI, and F4TCNQ:Li-TFSI with (w/) or without (w/o) photoexcitation. Electrical conductivity of PE-MD of PDPP4T films as a function of (e) white light intensity and (f) wavelength.

The HOMO level of the PDPP4T polymer (−5.12 eV) and the LUMO level of the well-studied dopant F4TCNQ (−5.24 eV) should facilitate efficient charge transfer in principle. However, F4TCNQ exhibits low doping efficiency when used to dope PDPP4T via conventional chemical doping or even ion-exchange doping techniques.[31] The PE-MD method, on the other hand, involves a sequential solution doping process, where the polymer films are immersed into dopant solutions followed by light excitation before the films are taken out (Figure 1b). As depicted in Figures 2a and S1, the doped PDPP4T films utilizing different doping methods were systematically characterized by employing ultraviolet−visible−near-infrared (UV−vis−NIR) absorption spectroscopy. For the PDPP4T films with sequential doping by F4TCNQ or F4TCNQ:Li-TFSI in the ground state (without photoexcitation), the two characteristic peaks of the pristine PDPP4T exhibit minimal change accompanied by only a slight increase in absorption in the longer wavelength region, indicating weak doping of PDPP4T. In contrast, the presence of light irradiation (photoexcitation) during the doping process results in the bleaching of the two typical neutral absorption peaks and the appearance of new peak(s) in the NIR region (above 900 nm), which is indicative of the formation of (bi)polaronic species and implies effective charge transfer between PDPP4T and the dopant.[21,22] This observation is corroborated by the significantly enhanced electron spin resonance (ESR) signals observed for PDPP4T films doped with F4TCNQ or F4TCNQ:Li-TFSI under photoexcitation, as opposed to those doped by using the conventional sequential doping method without photoexcitation (Figure 2b).

Ultraviolet and X-ray photoelectron spectroscopy (UPS and XPS) were performed to investigate the electron transfer interactions between PDPP4T and dopants.[37,38] Observations of shifts in both the high binding energy secondary electron cutoff and the low binding energy valence band feature toward lower binding energies indicate p-type doping characteristics for all doped films, as their Fermi levels are all shifted toward their HOMO level (Figure 2c). Notably, PDPP4T films doped in a photoexcited state exhibit a relatively significant larger work function and HOMO feature shifts compared to those doped in the ground state, signifying a more pronounced p-doping effect. The most substantial shift, indicative of the strongest doping level, is obtained in the PDPP4T film doped with F4TCNQ:Li-TFSI using the PE-MD method. Meanwhile, the UPS findings are consistent with the XPS results. For instance, the binding energy signals of C 1s, N 1s, and S $2p_{3/2}$ shift from 284.89, 400.11, and 164.39 eV, respectively, in the pristine PDPP4T film to lower binding energies in films doped in the ground state with F4TCNQ or F4TCNQ:Li-TFSI (Figure S2). A further shift toward lower binding energies is observed for films doped in the photoexcited state, pointing to an enhanced oxidation state of PDPP4T. Additionally, in the C 1s spectrum of the F4TCNQ-doped sample under photoexcitation, a new intense feature is observed at around 286.6 eV (Figure S2a), which can be attributed to the cyano-related signaling in enriched F4TCNQ within the sample after


https://doi.org/10.1021/jacsau.4c00567
JACS Au 2024, 4, 3884−3895

Table 1. Summary of the Electrical Conductivity ($\sigma$), Mobility ($\mu_{Hall}$), and Carrier Density ($n_{Hall}$) for the Indicated Polymers Doped by Selective Dopants without (w/o) or with (w/) Photoexcitation

| polymer | dopant | $\sigma$ (S cm$^{-1}$) w/o | $\sigma$ (S cm$^{-1}$) w/ | $\mu_{Hall}$ (cm$^2$ V$^{-1}$ s$^{-1}$) w/ | $n_{Hall}$ (cm$^{-3}$) w/ |
|---|---|---|---|---|---|
| PDPP4T | F2TCNQ:Li-TFSI | 0.005 ± 0.002 | 121.20 ± 14.79 | 1.25 ± 0.18 | (2.82 ± 0.09) × 10$^{20}$ |
| | F4TCNQ:Li-TFSI | 0.041 ± 0.012 | 337.85 ± 11.82 | 0.57 ± 0.12 | (2.20 ± 0.07) × 10$^{21}$ |
| | F6TCNNQ:Li-TFSI | 1.53 ± 0.21 | 268.51 ± 23.25 | 0.46 ± 0.17 | (2.91 ± 0.03) × 10$^{21}$ |
| | DDQ:Li-TFSI | 0.004 ± 0.002 | 89.54 ± 8.65 | 0.83 ± 0.03 | (4.40 ± 0.14) × 10$^{20}$ |
| PDPP3T | F4TCNQ:Li-TFSI | 0.014 ± 0.001 | 220.49 ± 16.45 | 0.32 ± 0.02 | (3.90 ± 0.13) × 10$^{21}$ |
| DPP-DTT | | 0.022 ± 0.001 | 260.51 ± 14.11 | 0.86 ± 0.03 | (1.67 ± 0.05) × 10$^{21}$ |
| IDTBT | | 0.00027 ± 0.00002 | 15.40 ± 1.78 | 1.68 ± 0.12 | (0.43 ± 0.01) × 10$^{20}$ |

doping.[39] However, in the S 2p spectrum of the F4TCNQ:Li-TFSI-doped sample under photoexcitation, a distinct new peak at around 167.9 eV is observed (Figure S2b), which is specifically indicative of the presence of the sulfonyl group of the TFSI$^-$ component.[40,41] The combination analysis of UPS and XPS spectra, together with the UV−vis−NIR absorption and ESR results, suggests that introduction of photoexcitation facilitates efficient p-doping of the PDPP4T polymer in a remarkable manner.

The $\sigma$ values of the doped PDPP4T films were determined using the four-probe method (Figure 2d). The maximum $\sigma$ values for the PDPP4T films doped in the ground state with F4TCNQ and F4TCNQ:Li-TFSI are measured to be merely 0.013 ± 0.004 and 0.041 ± 0.012 S cm$^{-1}$, respectively. In contrast, the introduction of photoexcitation during the doping process results in a substantial enhancement in $\sigma$, with the maximum values reaching 15.30 ± 2.01 and 337.85 ± 11.82 S cm$^{-1}$ for the PDPP4T films doped with F4TCNQ and F4TCNQ:Li-TFSI, respectively, achieving the highest value for ever-reported doped PDPP4T thin films.[42,43] The discrepant $\sigma$ of the doped PDPP4T by PE-MD with different dopants may stem from the influence of dopant counterions on the polymer's microstructure at a high doping density. Specifically, the attractive Coulomb forces between the charge carriers and the dopant ions can alter the polymer's microstructure, thereby affecting its $\sigma$.[44] In contrast, the closed-shell counterion TFSI$^-$ is less likely to interfere with the charge transport process, which promotes more efficient charge transport, resulting in enhanced $\sigma$ compared to the use of F4TCNQ alone.[28,31] Here, the PDPP4T film doped with F4TCNQ:Li-TFSI by the PE-MD process demonstrates superior stability compared to the traditional $FeCl_3$ immersing doped film, evidenced by continuously measuring their $\sigma$ in an air ambient environment (Figure S3). Notably, effective doping of PDPP4T can also be achieved using only Li-TFSI alone as a dopant under photoexcited conditions, yielding a maximum $\sigma$ of 3.5 S cm$^{-1}$. In this scenario, oxygen acts as an electron acceptor, while TFSI$^-$ serves as redox-inert counterions to stabilize the charges on the doped PDPP4T.[33,45] These results further substantiate the potential of the unique PE-MD method to achieve remarkably improved doping levels.

To assess the general applicability of the PE-MD approach, we extended our investigation to other representative dopants and D−A polymers (Figure S4a). 2,5-Difluoro-7,7,8,8-tetracyanoquinodimethane (F2TCNQ), 2,2′-(perfluoronaphthalene-2,6-diylidene) dimalononitrile (F6TCNNQ), and 2,3-dichloro-5,6-dicyano-*p*-benzoquinone (DDQ) were separately mixed with Li-TFSI in an acetonitrile solvent for PE-MD investigation. As shown in Table 1 and Figure S4b, the PE-MD of PDPP4T with F6TCNNQ:Li-TFSI in particular exhibits a conspicuous increase in $\sigma$. Even though F2TCNQ and DDQ have shallower LUMO levels (−5.03 and −4.81 eV, respectively)[46] compared to F4TCNQ and F6TCNNQ, the PE-MD approach still notably promotes the maximum $\sigma$ of doped PDPP4T to 121.20 ± 14.79 and 89.54 ± 8.65 S cm$^{-1}$, respectively. In addition, PE-MD doping of other copolymers, including poly[2,2′-[(2,5-bis(2-hexyldecyl)-3,6-dioxo-2,3,5,6-tetrahydropyrrolo[3,4-*c*]pyrrole-1,4-diyl)dithiophene]-5,5′-diyl-*alt*-thiophen-2,5-diyl] (PDPP3T), poly[2,5-(2-octyldodecyl)-3,6-diketopyrrolopyrrole-*alt*-5,5-(2,5-di(thien-2-yl)thieno-[3,2-*b*]thiophene)] (DPP-DTT), and indacenodithiophene-*co*-benzothiadiazole (IDTBT), were also examined. As expected, remarkable enhancements (>10$^4$ times) in $\sigma$ are achieved, with maximum values approaching 220.49 ± 16.45 and 260.51 ± 14.11 S cm$^{-1}$ for PDPP3T and DTT-DPP, respectively, when doped with F4TCNQ:Li-TFSI in a photoexcited state, contrasting sharply with samples doped in the ground state (Figure S4c and Table 1). Similarly, despite the HOMO level of IDTBT (−5.4 eV) being deeper than the LUMO level of the F4TCNQ dopant (−5.24 eV), the PE-MD process with F4TCNQ:Li-TFSI enables a maximum $\sigma$ of up to 15.40 ± 1.78 S cm$^{-1}$ for IDTBT, significantly surpassing the low doping level in the ground state showing only a $\sigma$ of ∼0.0003 S cm$^{-1}$. Furthermore, the carrier density ($n_{Hall}$) and mobility ($\mu_{Hall}$) of these doped films using PE-MD were assessed by employing Hall effect measurements. The results reveal a remarkably high $n_{Hall}$ of 0.43 × 10$^{20}$−3.90 × 10$^{21}$ m$^{-3}$, with $\mu_{Hall}$ in the range of 0.32−1.68 cm$^2$ V$^{-1}$ s$^{-1}$ (Table 1). These outcomes underscore the versatility and effectiveness of the PE-MD method across various D−A polymer systems.

To ascertain that the observed increase in the doping level is attributed to the photoexcitation effect of PE-MD rather than a photothermal effect, a control experiment based on the thermal effect was conducted. We evaluated the $\sigma$ of F4TCNQ:Li-TFSI-doped PDPP4T at various temperatures in the absence of photoexcitation (Figure S5). The results indicate that changes in sample temperature have a minimal impact on the doping level or $\sigma$ of PDPP4T, demonstrating that the photothermal effect is considerably less pronounced compared to the impact of photoexcitation.

To gain deep insights into the PE-MD mechanism, we examined the influence of light intensity and wavelength on the PE-MD levels. Our findings reveal that both the intensity and duration of light exposure significantly affect PE-MD efficiency, with $\sigma$ incrementally increasing with light intensity and exposure time increase (Figures 2e and S6). Notably, $\sigma$ reaches a plateau when the light intensity exceeds 100 mW cm$^{-2}$ or when the illumination time surpasses 10 min. Surprisingly, the doping level is tremendously enhanced under shorter wavelength photoexcitation, contrasting with the indistinctive improvement observed under red photoexcitation despite the fact that PDPP4T exhibits prominent


https://doi.org/10.1021/jacsau.4c00567
JACS Au 2024, 4, 3884−3895

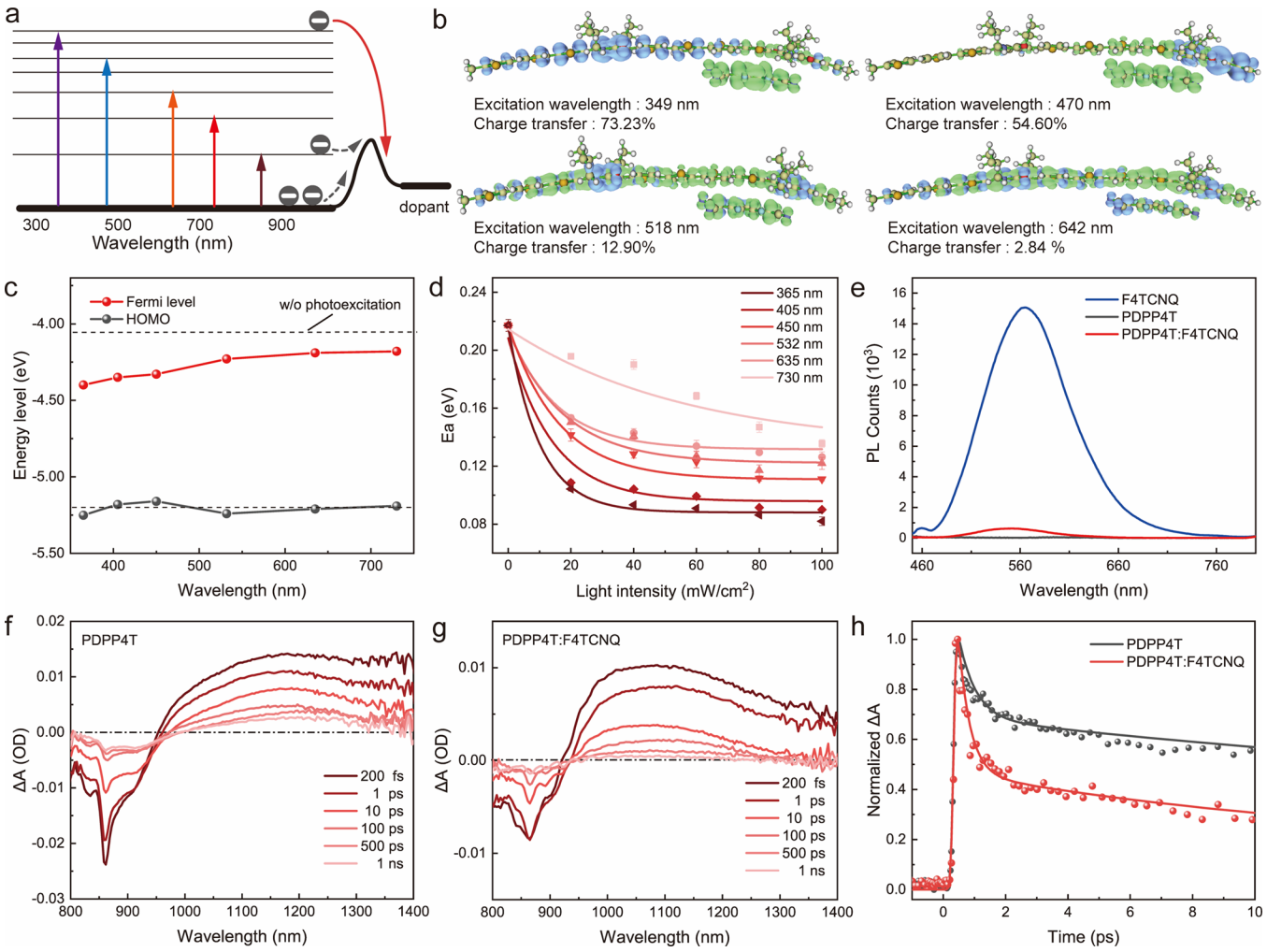


**Figure 3.** PE-MD mechanism. (a) Illustration of photoinduced electron transfer between the host polymer and the dopant under different wavelengths. (b) Optimized geometries and the distribution of holes (blue) and electrons (green) of the PDPP4T:F4TCNQ complex calculated by a TD-DFT method at the B3LYP/613G and analysis on the Multiwfn program. (c) Fermi level and HOMO of the PDPP4T film under excitation by different wavelengths. (d) Light intensity and wavelength-dependent activation energy of the PDPP4T film. (e) Photoluminescent spectra of F4TCNQ, PDPP4T, and PDPP4T:F4TCNQ under 370 nm excitation. Femtosecond transient absorption spectra of (f) PDPP4T and (g) PDPP4T:F4TCNQ complex excited by 370 nm. (h) Time-dependent normalized concentration of PDPP4T and PDPP4T:F4TCNQ film obtained from soft-modeling MCR-ALS analysis of the transient absorption data of 1180 nm with 370 nm excitation.

absorption in the long wavelength region of 600−900 nm (Figures 2f and S7). This discrepancy may be due to the higher energy photons with shorter wavelengths ensuring more efficient photoionization of PDPP4T, thereby resulting in a higher PE-MD level.[47] This trend is more intuitively manifested from the relationship between $\sigma$ and the excitation wavelength, irrespective of the dopant used. Moreover, the F4TCNQ dopant only displays distinct absorption peaks at around 330−420 nm, whereas Li-TSFI demonstrates almost no absorption in the visible region (Figure S8). These observations indicate that the PE-MD level is primarily dependent on the energy of photoexcitation rather than the absorption characteristics of the host polymer or the dopant.

## 2.2. Mechanism of PE-MD

The wavelength-dependent PE-MD process can be attributed to the disparity between the ionization energy (IP) and electron affinity (EA) of the polymer in its ground and excited states. In the photoexcited state, the excitation energy ($h\nu$) is associated with the ionization potential (IP*) and electron affinity (EA*) of excited molecules through the following relation: EA* = EA + $h\nu$ and IP* = IP − $h\nu$.[48] Molecules in an excited state are more prone to charge transfer compared with those in the ground state, a phenomenon driven by increased chemical reactivity that is also contingent upon the energy of the incident photons. As depicted in Figure 3a, the low-energy electrons generated by photoexcitation at long wavelengths may not have sufficient $E_a$* to effectively transfer into the dopant molecule, thereby affecting the efficiency of the charge transfer process.

To provide further clarity on the intermolecular P-ET process between PDPP4T and F4TCNQ, we conducted density functional theory (DFT) and time-dependent DFT (TD-DFT) calculations (Figure S9).[49] These computational approaches were complemented by an examination of the excited-state electron transfer properties of the PDPP4T:F4TCNQ complex using the interfragmentary charge transfer method based on the Multiwfn program (Figures 3b and S10).[50] To identify the most stable doping site, we carefully performed geometric optimization and energy calculations for different potential site configurations, as


https://doi.org/10.1021/jacsau.4c00567
JACS Au 2024, 4, 3884−3895

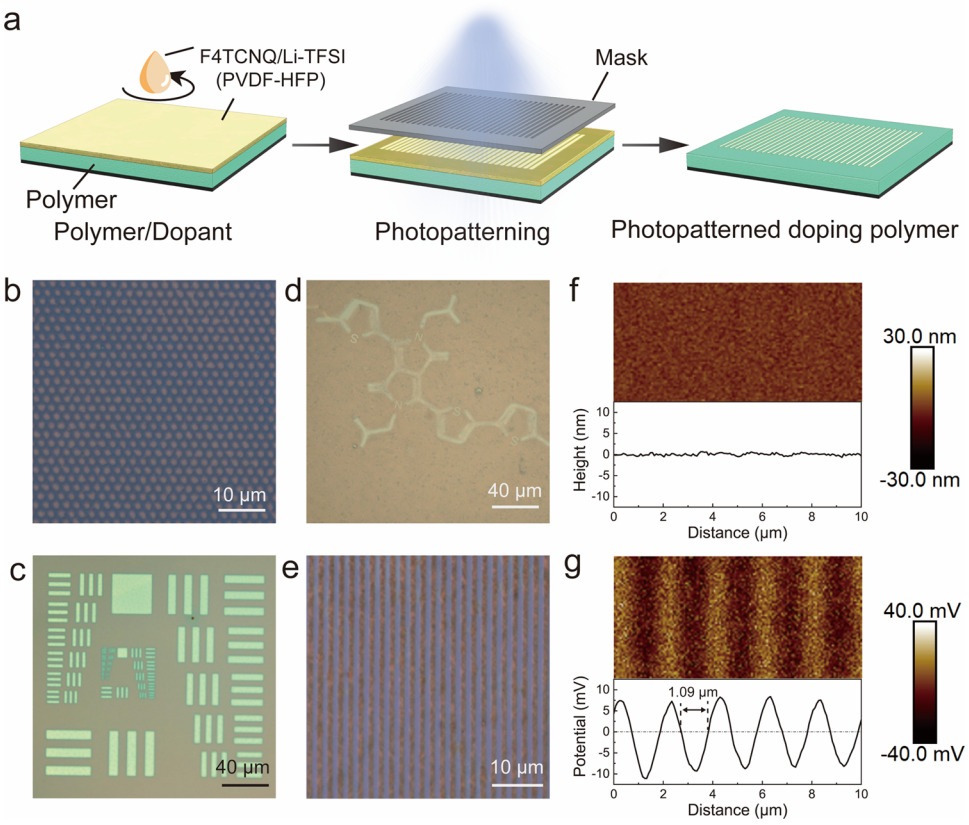


**Figure 4.** Photopatterning of doped PDPP4T through PE-MD. (a) Photopatterned doping process. Optical microscope images of various doped patterns, including (b) dots with a diameter of 1 $\mu$m, (c) 1951 USAF resolution test chart clines, (d) molecular structure of PDPP4T, and (e) lines with a width of 1 $\mu$m. (f) AFM surface and (g) KPFM images of patterned doped lines with a width of 1 $\mu$m.

illustrated in Figure S11. Among these, the configuration depicted in Figure S11d, situated on the thiophene ring, exhibits the lowest energy. This finding suggests that it is the most thermodynamically stable configuration. Based on this molecular conformation and the relative position, we subsequently conducted an intermolecular charge transfer calculation. The distribution of electrons and holes within the PDPP4T:F4TCNQ complex at varying excitation wavelengths was calculated, revealing that at low-energy (long-wavelength) photoexcited states, the electron cloud (green) is predominantly localized within PDPP4T. However, as the photoexcitation energy increases, the electron cloud progressively shifts toward the F4TCNQ dopant, concurrent with an expanding hole cloud (blue) in PDPP4T. This shift is accompanied by an elevated rate of charge transfer between PDPP4T and F4TCNQ, which aligns with the observed wavelength-dependent $\sigma$ for PE-MD of PDPP4T (Figure S10). The larger shift of the Fermi level toward the HOMO at a higher excitation energy, as indicated by the wavelength-dependent UPS results for PDPP4T (Figures 3c and S12), also suggests an increase in photogenerated holes, indicating a greater propensity for electrons to be excited under short-wavelength photoexcitation.[47] This increase in the number of excited electrons is believed to enhance the probability of P-ET, thereby contributing to the improved p-doping level of PDPP4T.

The underlying mechanism of the PE-MD effect was further substantiated through hopping $E_a$ analysis, which reveals the minimum energy threshold necessary to initiate a chemical reaction. $E_a$ is derived from fitting the empirical relationship $\sigma = \sigma_0 e^{-E_a/k_BT}$, where $\sigma_0$, $k_B$, and $T$ are the temperature-independent preexponential factor, the Boltzmann constant, and temperature, respectively.[51,52] The temperature-dependent lateral $\sigma$ of the pristine PDPP4T thin film was measured under different wavelengths and intensities (Figure S13). As indicated in Figure 3d, a more pronounced reduction in $E_a$ is observed with an increase in light intensity and a decrease in light wavelength. This reduction in $E_a$ substantiates the notion that high-energy photons are more effective in generating photoinduced holes in PDPP4T, concurrently increasing the population of excited-state electrons.

To further elucidate the mechanism underlying PE-MD, photoluminescence (PL) and femtosecond transient absorption (fs-TA) spectroscopy were employed to examine the deactivation pathways of the excited states. As illustrated in Figure 3e, F4TCNQ exhibits strong fluorescence within the 460−660 nm range when excited at 370 nm, whereas PDPP4T exhibits negligible fluorescence under the same condition. The hybridization of F4TCNQ with PDPP4T results in significant quenching of the fluorescence of F4TCNQ. This quenching suggests the occurrence of substantial charge transfer between PDPP4T and F4TCNQ, which in turn reduces the probability of exciton recombination, leading to diminished PL intensity in F4TCNQ.[53]

Employing a 370 nm femtosecond pulse for excitation, we recorded fs-TA spectra at various pump−probe delays in the NIR region, ranging from 800 to 1400 nm. Photoexcitation of the pristine PDPP4T film yields a broad excited-state absorption peak at around 1180 nm (Figure 3f), likely due to the spectral overlap of exciton features and the intra-


https://doi.org/10.1021/jacsau.4c00567
JACS Au 2024, 4, 3884−3895

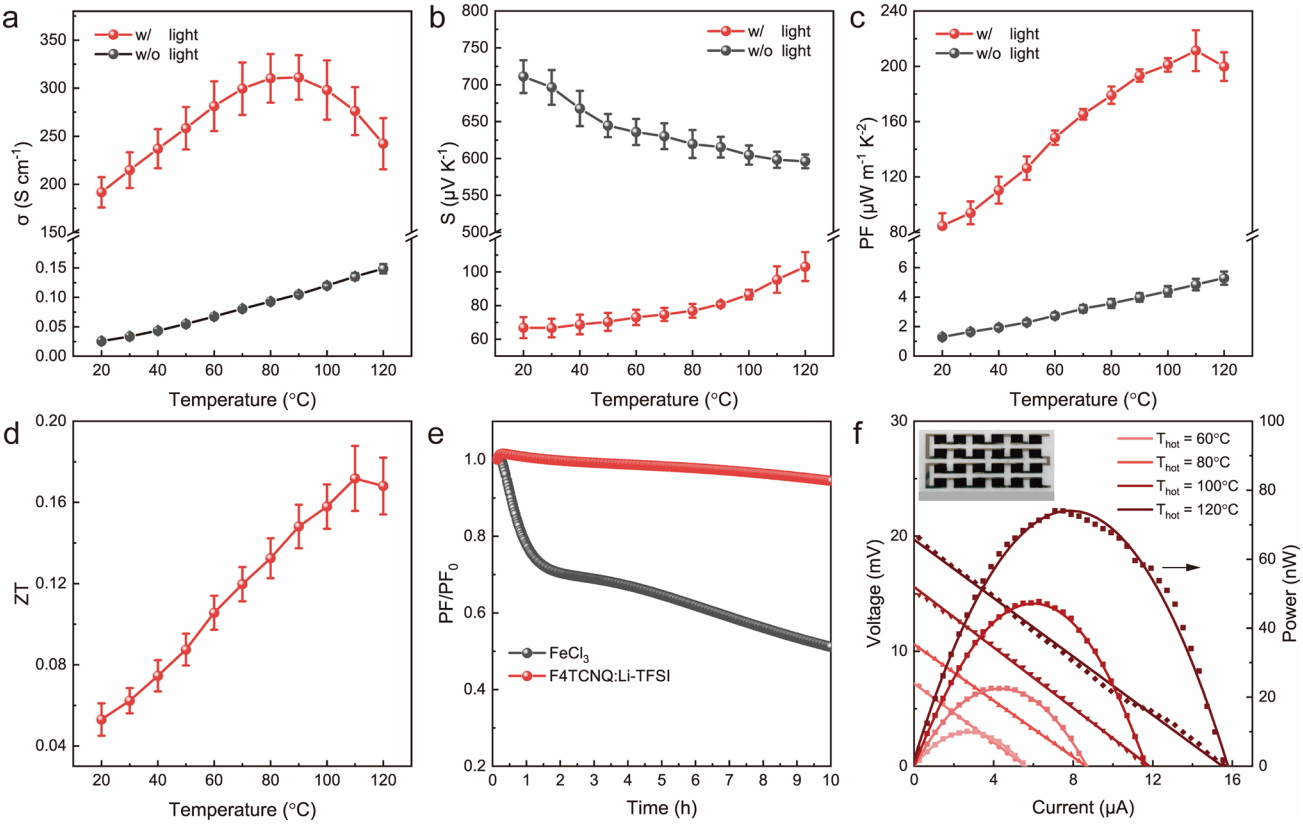


**Figure 5.** TE performance of doped PDPP4T. Temperature-dependent (a) electrical conductivity, (b) Seebeck coefficient, (c) PF, and (d) *ZT* of the PDPP4T films doped with or without photoexcitation. (e) PF changes versus heating treatment time at 100 °C in PDPP4T films doped with F4TCNQ:Li-TFSI by PE-MD and $FeCl_3$ by immersing doping. (f) Output voltage and power of the OTE generator at different heat source temperatures (under the ambient temperature of 25 °C).

molecular charge transfer transition characteristic of its D−A structure.[54,55] In contrast, the PDPP4T:F4TCNQ complex shows a blue shift of the absorption peak to around 1080 nm (Figure 3g), indicative of ion formation accompanied by the occurrence of charge transfer.[54] Time-resolved analysis at 1180 nm for the pristine PDPP4T film reveals three time constants: 519 fs, 23 ps, and 2663 ps (Figures 3h and S14). The shortest lifetime of 519 fs corresponds to the evolution of the exciton to a partial charge transfer state within the D−A units. The longer lifetimes should be attributed to the relaxation of the intrachain/interchain charge transfer state.[54,56] In contrast, the PDPP4T:F4TCNQ blend film exhibits shorter decay times: 230 fs, 18 ps, and 2477 ps, indicating a faster exciton decay process. The shortened decay time, particularly in the 230 fs state, is attributed to the occurrence of a new fast competing pathway on the exciton state that is ascribed to the intermolecular charge transfer between PDPP4T and F4TCNQ.[56,57] Thus, the rapid decay of transient absorption in the PDPP4T:F4TCNQ complex under photoexcitation signifies the efficient doping of PDPP4T.

### 2.3. Photopatterned Doping of PDPP4T

A crucial aspect of organic active layers in organic electronics involves the construction of functional devices through patterning techniques. Photolithography stands out as a highly refined technology, renowned for its high spatial resolution and its capacity to produce large-area integrated devices.[58−61] In this study, we propose an innovative method for patterning doped PSCs that integrates PE-MD with photolithography. The dopants F4TCNQ and Li-TFSI were mixed and dissolved in poly(vinylidene fluoride-*co*-hexafluoropropylene) (PVDF-HFP) in an n-butyl acetate solution. This solvent mixture was selected for its favorable attributes, including mechanical stability, high dielectric constant, low degree of crystallinity, and high ionic conductivity, all of which promote the efficient dissociation of salts.[62] Figure 4a provides a visual representation of the patterning doping process, where the PVDF-HFP solution containing the F4TCNQ:Li-TFSI dopant mixture was spin-coated onto the PDPP4T film, followed by fitting a mask intimately against the sample surface. Utilizing 100 mW $cm^{-2}$ of 365 nm ultraviolet light for excitation, we achieved high-resolution patterned doping with features on the order of 1 $\mu$m. The low surface energy of PVDF-HFP enabled its facile stripping off from the PDPP4T surface.[63] Although the solid-state PE-MD process applied to PDPP4T involves a discrepancy due to the potentially restricted movement of dopants within the solid PVDF-HFP matrix compared to the PE-MD process in solution, it still achieves an impressively high $\sigma$, reaching a maximum value of 106.30 ± 1.23 S $cm^{-1}$ under 13 min of illumination (Figure S15).

Based on the above-mentioned patterning doping process, various high-resolution patterns featuring both doped and undoped regions were successfully achieved. These patterns include individual dots with dimensions of 1 $\mu$m (the minimum mask size we used; Figure 4b), the USAF resolution test chart (Figure 4c), a representation of the molecular structure of PDPP4T (Figure 4d), and individual lines with a mask width of 1 $\mu$m (Figure 4e). Atomic force microscopy (AFM) and Kelvin probe force microscopy (KPFM) were


https://doi.org/10.1021/jacsau.4c00567
JACS Au 2024, 4, 3884−3895

performed to characterize the surface properties and the resolution of the patterned doping. The AFM result for the patterned doping sample with individual 1 $\mu$m lines of Figure 4e reveals a rather smooth surface (Figure 4f), indicating that the PVDF-HFP/dopant layer is entirely removed without disrupting subsequent processes. The KPFM image of the same sample distinctly delineated the doped and undoped regions of the lines, demonstrating that the patterned doping resolution can achieve 1 $\mu$m with a lateral extended doping length of lower than 100 nm (Figure 4g).[63] We highlight here that this solid-state PE-MD doping method can also be effectively implemented by using a high-intensity, well-focused direct laser writing source for excitation. This approach offers a preferable doping resolution and eliminates the need for a mask, thereby enhancing the precision of the process.[64,65]

Leveraging the effective PE-MD process and its high spatial-resolution patterning capabilities, we proceeded to fabricate a polymer FET. This FET featured photoexcitation-assisted molecularly doped PDPP4T (using the optimized $\sigma$ condition) as the source and drain electrodes, with the left undoped PDPP4T channel serving as the active layer on a $Si^{2+}/SiO_2$ substrate (Figure S16a). The FET demonstrates smooth transfer and output characteristics, indicative of p-channel transport behavior (Figure S16b,c). The data analysis yields an average FET mobility of 0.24 $cm^2\ V^{-1}\ s^{-1}$ for this device, a value that is comparable to the performance of a device utilizing conventional Au source/drain electrodes (0.44−3.13 $cm^2\ V^{-1}\ s^{-1}$).[52] The observed discrepancy may be due to the relatively lower local $\sigma$ of the PDPP4T electrodes doped by the PE-MD method when compared with the Au electrodes. Nonetheless, the PE-MD approach provides a potential route to develop all-polymer-based electronic devices with patterned electrodes, offering significant potential for the rapid and facile fabrication of flexible integrated circuits.

### 2.4. TE Performance of PDPP4T Doped via PE-MD

The high PE-MD efficiency with high carrier density should facilitate efficient TE conversion. We characterized the $\sigma$ and Seebeck coefficient ($S$) of PDPP4T films doped via PE-MD to evaluate their TE performance. For the F4TCNQ:Li-TFSI-doped PDPP4T films, $\sigma$ is found to increase with the doping time, regardless of the presence of photoexcitation (Figure S17a). A maximum $\sigma$ of 337.85 ± 11.82 S $cm^{-1}$ is achieved at a photoexcitation doping time of around 14 min, making an over 4-order of magnitude increase compared to the sample without photoexcitation (~0.02 S $cm^{-1}$). Prolonging the photoexcitation doping time leads to a decrease in $\sigma$, likely due to alterations in molecular packing.[21] In terms of the $S$, films doped without or with photoexcitation exhibit similar decreasing trends. The values decline steadily from 941 ± 25 or 144.5 ± 6.7 to 710 ± 21 or 41.0 ± 3.9 $\mu V\ K^{-1}$, respectively, as the doping time is extended from 4 to 16 min (Figure S17b). The PE-MD sample achieves a maximum PF of 101.3 ± 3.9 $\mu W\ m^{-1}\ K^{-2}$ at a doping time of 12 min at room temperature, which is nearly 2 orders of magnitude higher than that of the PDPP4T doped without photoexcitation (Figure S17c).

In addition, we examined the temperature-dependent TE properties of the PDPP4T film doped under optimal PE-MD conditions with an optimized PF. The thermally assisted activation process leads to a pronounced temperature-dependent increase in $\sigma$, which gradually rises with elevated temperature, reaching a maximum of 311.1 ± 23.1 S $cm^{-1}$ at approximately 80 °C (Figure 5a). Further increase in temperature results in a decreased $\sigma$ due to the dedoping process. The $S$ also exhibits a significant increase, from 66.5 ± 5.5 to 103.2 ± 8.6 $\mu V\ K^{-1}$ for the PE-MD film (Figure 5b). In contrast, the $\sigma$ of PDPP4T doped without photoexcitation continuously increases with temperature, exhibiting a typical hopping transport behavior, yet its $S$ decreases with temperature. This behavior can be attributed to the reduced nearest neighbor hopping thermopower at elevated temperatures for low doping level samples.[66] As a result, the PDPP4T doped without photoexcitation achieves a maximum PF of only 5.29 ± 0.44 $\mu W\ m^{-1}\ K^{-2}$ due to its substantially lower $\sigma$. In stark comparison, by exploiting the temperature-dependent characteristics, the PE-MD-treated sample attains a maximum PF of 211.3 ± 14.8 $\mu W\ m^{-1}\ K^{-2}$ at 110 °C. To thoroughly assess the TE performance, we employed a thin-film analyzer (TFA, Linseis)[67] to measure the in-plane thermal conductivity ($\kappa_{\parallel}$) of the PE-MD-treated PDPP4T film (Figure S18). Unlike the cases of $\sigma$ and $S$, $\kappa_{\parallel}$ exhibits minimal temperature dependence across the range of 20−120 °C. Consequently, the PE-MD-treated PDPP4T demonstrates a maximum $ZT$ value of 0.16 ± 0.02 at around 110 °C (Figure 5d).

Furthermore, the PE-MD films exhibit exceptional TE stability when compared to the extensively investigated $FeCl_3$ doping method (Figures 5e and S19). For instance, the PF of the PDPP4T film doped by the PE-MD method experiences minimal decay of less than 5%, even though its $\sigma$ reduces to 75% after 10 h of continuous heating at 100 °C, which is concomitant with an increase in $S$ to ~110%. In contrast, even though the $S$ of the sample doped by $FeCl_3$ using a conventional immersion doping method boosts to nearly 2.2 times its initial value after the same heating period at 100 °C via the $\sigma$−$S$ constrained relationship, the PF for this sample is only retained at about 50% because $\sigma$ drops dramatically to just 10%. The results indicate that the PE-MD method can significantly enhance doping stability compared to the traditional chemical doping method.

Capitalizing on the solution processability, patternability, high stability, and prominent TE performance of PDPP4T doped by the PE-MD method, we fabricated a flexible all-polymer TE generator. The PDPP4T doped by F4TCNQ:Li-TFSI using the PE-MD method served as the p-leg element, while the commercially available and solution-processable poly(benzodifurandione) (PBFDO) was employed as the n-leg element.[68,69] For the TE generator fabrication, PDPP4T and PBFDO were initially patterned through drop-casting on a flexible poly(ethylene terephthalate) substrate. Subsequently, a PVDF-HFP solution containing F4TCNQ and Li-TFSI was coated on the p−n module, followed by selective doping of the PDPP4T legs using an exposure mask by the PE-MD method. The remaining F4TCNQ:Li-TFSI-containing PVDF-HFP layer was then removed through stripping it off. The resulting flexible TE generator was folded into a corrugated shape and tested on a hot plate under ambient conditions (Figures S20 and S21). The actual temperature gradient across the generator can be calibrated by temperature sensors (Figure S22). Upon heating the hot plate to 120 °C, which established a temperature difference $\Delta T$ = 27 °C between the hot and cold ends at 64.8 and 37.8 °C, respectively, the generator produced an open-circuit voltage of 20.1 mV and a short-circuit current of 15.8 $\mu$A, culminating in a maximum power output of 74 nW (Figure 5f). The result underscores the


https://doi.org/10.1021/jacsau.4c00567
JACS Au 2024, 4, 3884−3895

potential of the efficient PE-MD polymer in the development of all-polymer flexible TE generators.

## 3. CONCLUSIONS

In summary, we present an effective strategy that significantly enhances the doping level of D−A copolymers through the PE-MD approach. This method capitalizes on the principle of P-ET in the photoexcited state, allowing for a high p-doping level even with dopants featuring shallow EA. This contrasts with conventional p-type doping methods, which typically require dopants with a deep LUMO level. The PE-MD method provides a viable route for achieving high-resolution patterned doping of PSCs, showcasing its potential for use in patterned electrodes for polymer FETs. Furthermore, the efficient PE-MD of PDPP4T enables a maximum PF of 226.1 $\mu$W m$^{-1}$ K$^{-2}$, which in turn contributes to a notable $ZT$ of 0.18. These findings pave the way for possibilities in achieving high doping levels in polymers, facilitating the development of easy-to-process patterned devices and high-performance polymeric TE materials.

## 4. EXPERIMENTAL SECTION

### 4.1. Materials

PDPP4T, IDTBT, DPP-DTT, and PDPP3T were purchased from Solarmer Material (Beijing) Inc. F2TCNQ (>99%), F4TCNQ (>99%), and F6TCNNQ (>99%) were purchased from TCI Chemical. Li-TFSI (>99%, <1% water) was purchased from Sigma-Aldrich. PVDF-HFP was purchased from 3M. All of these materials were used as received without any purification.

### 4.2. Device Fabrication and Doping Methodology

PDPP4T, DPP-DTT, and IDTBT PSCs (10 mg/mL) were dissolved in chloroform, whereas PDPP3T (10 mg/mL) was dissolved in 1,2-dichlorobenzene and was heated at 80 °C to improve its solubility.

Dopant solutions were prepared by individually dissolving F4TCNQ (5 mg/mL), DDQ (5 mg/mL), F2TNCQ (5 mg/mL), and F6TCNNQ (5 mg/mL) in acetonitrile. Additionally, Li-TFSI (30 mg/mL) was codissolved with these dopants in acetonitrile. The PSCs were doped simply by immersing their solid-state thin films into the dopant solutions, under either dark conditions or light illumination.

For TE property investigation, glass substrates were ultrasonically cleaned with deionized water, alcohol, and acetone in sequence. The Cr/Au (5/30 nm) patterned parallel electrodes were thermally evaporated in a vacuum using a shadow mask with a channel length of 500 $\mu$m and a channel width of 5000 $\mu$m for lateral electrical conductivity and Seebeck coefficient measurements. The semiconducting polymer solutions were then spin-coated onto the cleaned substrates at 3000 rpm for 60 s. All films were annealed at 100 °C for 1 h in a nitrogen-filled glovebox.

### 4.3. Photopatterned Doping Procedure

The dopant solution was prepared by codissolving PVDF-HFP (100 mg/mL), F4TCNQ (0.01 mg/mL), and Li-TFSI (0.5 mg/mL) in $N$-butyl acetate. This solution was then spin-coated onto PDPP4T at a speed of 3000 rpm. A mask was closely applied to the sample, followed by exposure to 365 nm UV light (100 mW cm$^{-2}$) for patterned doping.

### 4.4. Transistor, Thermoelectric, and Hall Effect Performance Characterization

The transfer and output characteristics of the FET were measured using an Agilent B2902A system in ambient conditions. The four-probe method was performed to determine the electrical resistivity with the Agilent B2902A and the Keithley 2182A. The Seebeck coefficient was calculated by $S = \Delta V/\Delta T$, where $\Delta V$ is the thermal voltage between two electrodes when applying a temperature difference $\Delta T$. The $\Delta V$ was measured with the Keithley 2182A within a homemade vacuum chamber. $\Delta T$ was generated by Peltier elements and calibrated based on the known relationship between resistance and temperature. The in-plane thermal conductivity was assessed using a thin-film analyzer (TFA, Linseis). The carrier density and mobility of the samples doped using the PE-MD method were analyzed through Hall effect measurements. Van der Pauw structured Hall devices were tested by using a Lakeshore FastHall system.

### 4.5. UPS and XPS Measurements

The UPS and XPS measurements were performed on an Axis Ultra DLD (Kratos, UK) spectrometer with an unfiltered He-discharge lamp (21.22 eV) and a monochromatic Al K$\alpha$ X-ray (1486.6 eV) as the excitation sources, respectively. A bias voltage of −9 V was applied to the sample for correctly obtaining the secondary electrons cutoff region. The Fermi level position of the spectra was calibrated to that of an Ar$^+$ ion sputtered clean gold foil. The PDPP4T thin films were spin-coated onto ultrasonically cleaned ITO glass substrates for simultaneous UPS and XPS measurements due to the stricter requirements of sample conductivity for UPS experiments.

### 4.6. Ultraviolet−Visible−Near-Infrared (UV−vis−NIR) Absorption and Photoluminescent Spectroscopy

The UV−vis−NIR absorption of pristine and doped PDPP4T, F4TCNQ, and Li-TFSI films on quartz glass substrates were recorded on a JASCO V-570 spectrometer. The PL spectra of PDPP4T, F4TCNQ, and PDPP4T:F4TCNQ complex on quartz glass substrates were performed on a fluorescence spectrophotometer (Edinburgh Instruments Spectrofluorometer FS5) under 370 nm excitation.

### 4.7. AFM and KPFM Characterization

The AFM image was obtained using a Bruker Dimension ICON FastScan microscope in the tapping mode. KPFM measurement was performed in ambient conditions using the same Bruker FastScan AFM instrument in the PeakForce KPMF mode. The scanning rate for the KPFM measurements was maintained at 16 Hz.

### 4.8. Femtosecond Transient Absorption (fs-TA) Spectroscopy

The fs-TA setup is composed of a regenerative-amplified Ti:sapphire laser system (Coherent) and a Helios pump−probe system (Ultrafast Systems). The regenerative-amplified Ti:sapphire laser system (Legend Elite-1K-HE, center wavelength of 800 nm, pulse duration of 25 fs, pulse energy of 4 mJ, and repetition rate of 1 kHz) was seeded with a mode-locked Ti:sapphire laser system (Vitara) and pumped with a Nd:YLF laser (Evolution 30). The excitation energy of the pump pulse was set to 2 $\mu$J cm$^{-2}$ to avoid singlet−singlet annihilation. The thin-film samples for fs-TA measurements were prepared by spin-coating the corresponding materials on thin quartz plates and thermally annealed in the same way as for the actual device.

## ■ ASSOCIATED CONTENT

### Supporting Information

The Supporting Information is available free of charge at https://pubs.acs.org/doi/10.1021/jacsau.4c00567.

Chemical structure of the materials used; UV−vis−NIR absorption spectra, XPS and UPS spectra, fs-TA spectra, electrical conductivity, stability, Seebeck coefficient, PF, and thermal conductivity of the doped films; theoretical calculated frontier orbital distribution of PDPP4T, relative energy, and charge transfer ratio between PDPP4T and F4TCNQ; image and transfer/output curves of the FET device; fabrication process, graphs of heating, and output of the TE generator (PDF)



https://doi.org/10.1021/jacsau.4c00567
JACS Au 2024, 4, 3884−3895

## AUTHOR INFORMATION


### Corresponding Authors

**Ye Zou** − *Beijing National Laboratory for Molecular Sciences, CAS Key Laboratory of Organic Solids, Institute of Chemistry, Chinese Academy of Sciences, Beijing 100190, China*; Email: zouye@iccas.ac.cn

**Chong-an Di** − *Beijing National Laboratory for Molecular Sciences, CAS Key Laboratory of Organic Solids, Institute of Chemistry, Chinese Academy of Sciences, Beijing 100190, China*; orcid.org/0000-0002-6183-1321; Email: dicha@iccas.ac.cn

### Authors

**Zhen Ji** − *Beijing National Laboratory for Molecular Sciences, CAS Key Laboratory of Organic Solids, Institute of Chemistry, Chinese Academy of Sciences, Beijing 100190, China; School of Chemical Sciences, University of Chinese Academy of Sciences, Beijing 100049, China*

**Zhiyi Li** − *Beijing National Laboratory for Molecular Sciences, CAS Key Laboratory of Organic Solids, Institute of Chemistry, Chinese Academy of Sciences, Beijing 100190, China*

**Xiaojuan Dai** − *Beijing National Laboratory for Molecular Sciences, CAS Key Laboratory of Organic Solids, Institute of Chemistry, Chinese Academy of Sciences, Beijing 100190, China*

**Lanyi Xiang** − *School of Chemical Sciences, University of Chinese Academy of Sciences, Beijing 100049, China*

**Yue Zhao** − *Beijing National Laboratory for Molecular Sciences, CAS Key Laboratory of Organic Solids, Institute of Chemistry, Chinese Academy of Sciences, Beijing 100190, China; School of Chemical Sciences, University of Chinese Academy of Sciences, Beijing 100049, China*

**Dongyang Wang** − *Beijing National Laboratory for Molecular Sciences, CAS Key Laboratory of Organic Solids, Institute of Chemistry, Chinese Academy of Sciences, Beijing 100190, China; School of Chemical Sciences, University of Chinese Academy of Sciences, Beijing 100049, China*

**Xiao Zhang** − *Beijing National Laboratory for Molecular Sciences, CAS Key Laboratory of Organic Solids, Institute of Chemistry, Chinese Academy of Sciences, Beijing 100190, China; School of Chemical Sciences, University of Chinese Academy of Sciences, Beijing 100049, China*

**Liyao Liu** − *Beijing National Laboratory for Molecular Sciences, CAS Key Laboratory of Organic Solids, Institute of Chemistry, Chinese Academy of Sciences, Beijing 100190, China*

**Zhiyuan Han** − *Beijing National Laboratory for Molecular Sciences, CAS Key Laboratory of Organic Solids, Institute of Chemistry, Chinese Academy of Sciences, Beijing 100190, China; School of Chemical Sciences, University of Chinese Academy of Sciences, Beijing 100049, China*

**Lixin Niu** − *Beijing National Laboratory for Molecular Sciences, CAS Key Laboratory of Organic Solids, Institute of Chemistry, Chinese Academy of Sciences, Beijing 100190, China; School of Chemical Sciences, University of Chinese Academy of Sciences, Beijing 100049, China*

**Yuqiu Di** − *Beijing National Laboratory for Molecular Sciences, CAS Key Laboratory of Organic Solids, Institute of Chemistry, Chinese Academy of Sciences, Beijing 100190, China; School of Chemical Sciences, University of Chinese Academy of Sciences, Beijing 100049, China*

**Daoben Zhu** − *Beijing National Laboratory for Molecular Sciences, CAS Key Laboratory of Organic Solids, Institute of Chemistry, Chinese Academy of Sciences, Beijing 100190, China*; orcid.org/0000-0002-6354-940X

Complete contact information is available at: https://pubs.acs.org/10.1021/jacsau.4c00567


### Notes

The authors declare no competing financial interest.

## ACKNOWLEDGMENTS

This work was financially supported by the National Natural Science Foundation of China (22175186, 22125504, U22A6002, 22305253, and 22021002), the Natural Science Foundation of Beijing (Z220025), the Strategic Priority Research Program of the Chinese Academy of Sciences (XDB0520200), and the Beijing National Laboratory for Molecular Sciences (BNLMS-CXXM-202402).

## REFERENCES


(1) Zhao, W.; Ding, J.; Zou, Y.; Di, C. A.; Zhu, D. Chemical doping of organic semiconductors for thermoelectric applications. *Chem. Soc. Rev.* **2020**, *49*, 7210−7228.

(2) Yu, Z.-D.; Lu, Y.; Wang, Z.-Y.; Un, H.-I.; Zelewski, S. J.; Cui, Y.; You, H.-Y.; Liu, Y.; Xie, K.-F.; Yao, Z.-F.; He, Y.-C.; Wang, J.-Y.; Hu, W.-B.; Sirringhaus, H.; Pei, J. High n-type and p-type conductivities and power factors achieved in a single conjugated polymer. *Sci. Adv.* **2023**, *9*, No. eadf3495.

(3) Scaccabarozzi, A. D.; Basu, A.; Anies, F.; Liu, J.; Zapata-Arteaga, O.; Warren, R.; Firdaus, Y.; Nugraha, M. I.; Lin, Y.; Campoy-Quiles, M.; Koch, N.; Muller, C.; Tsetseris, L.; Heeney, M.; Anthopoulos, T. D. Doping Approaches for Organic Semiconductors. *Chem. Rev.* **2022**, *122*, 4420−4492.

(4) Chen, Q.; Huang, H.; Hu, D.; Zhang, C. E.; Xu, X.; Lu, H.; Wu, Y.; Yang, C.; Bo, Z. Improving the Performance of Layer-by-Layer Processed Organic Solar Cells via Introducing a Wide-Bandgap Dopant into the Upper Acceptor Layer. *Adv. Mater.* **2023**, *35*, No. 2211372.

(5) Zhao, Y.; Wang, W.; He, Z.; Peng, B.; Di, C.-A.; Li, H. High-performance and multifunctional organic field-effect transistors. *Chin. Chem. Lett.* **2023**, *34*, No. 108094.

(6) Zhang, F.; Mohammadi, E.; Qu, G.; Dai, X.; Diao, Y. Orientation-Dependent Host−Dopant Interactions for Manipulating Charge Transport in Conjugated Polymers. *Adv. Mater.* **2020**, *32*, No. 2002823.

(7) Yan, H.; Ma, W. Molecular Doping Efficiency in Organic Semiconductors: Fundamental Principle and Promotion Strategy. *Adv. Funct. Mater.* **2021**, *32*, No. 2111351.

(8) Jacobs, I. E.; Moulé, A. J. Controlling molecular doping in organic semiconductors. *Adv. Mater.* **2017**, *29*, No. 1703063.

(9) Yuan, D.; Liu, W.; Zhu, X. Efficient and air-stable n-type doping in organic semiconductors. *Chem. Soc. Rev.* **2023**, *52*, 3842−3872.

(10) Luo, S.; Xu, Z.; Zhong, F.; Li, H.; Chen, L. Doping-induced charge transfer in conductive polymers. *Chin. Chem. Lett.* **2024**, *35*, No. 109014.

(11) Salzmann, I.; Heimel, G.; Oehzelt, M.; Winkler, S.; Koch, N. Molecular Electrical Doping of Organic Semiconductors: Fundamental Mechanisms and Emerging Dopant Design Rules. *Acc. Chem. Res.* **2016**, *49*, 370−378.

(12) Jacobs, I. E.; Lin, Y.; Huang, Y.; Ren, X.; Simatos, D.; Chen, C.; Tjhe, D.; Statz, M.; Lai, L.; Finn, P. A.; Neal, W. G.; D'Avino, G.; Lemaur, V.; Fratini, S.; Beljonne, D.; Strzalka, J.; Nielsen, C. B.; Barlow, S.; Marder, S. R.; McCulloch, I.; Sirringhaus, H. High-Efficiency Ion-Exchange Doping of Conducting Polymers. *Adv. Mater.* **2022**, *34*, No. 2102988.

(13) Kiefer, D.; Kroon, R.; Hofmann, A. I.; Sun, H.; Liu, X.; Giovannitti, A.; Stegerer, D.; Cano, A.; Hynynen, J.; Yu, L.; Zhang, Y.; Nai, D.; Harrelson, T. F.; Sommer, M.; Moule, A. J.; Kemerink, M.; Marder, S. R.; McCulloch, I.; Fahlman, M.; Fabiano, S.; Muller, C. Double doping of conjugated polymers with monomer molecular dopants. *Nat. Mater.* **2019**, *18*, 149−155.
(14) Kang, K.; Watanabe, S.; Broch, K.; Sepe, A.; Brown, A.; Nasrallah, I.; Nikolka, M.; Fei, Z.; Heeney, M.; Matsumoto, D.; Marumoto, K.; Tanaka, H.; Kuroda, S.-I.; Sirringhaus, H. 2D coherent charge transport in highly ordered conducting polymers doped by solid state diffusion. *Nat. Mater.* **2016**, *15*, 896−902.
(15) Karpov, Y.; Erdmann, T.; Raguzin, I.; Al-Hussein, M.; Binner, M.; Lappan, U.; Stamm, M.; Gerasimov, K. L.; Beryozkina, T.; Bakulev, V.; Anokhin, D. V.; Ivanov, D. A.; Günther, F.; Gemming, S.; Seifert, G.; Voit, B.; Di Pietro, R.; Kiriy, A. High Conductivity in Molecularly p-Doped Diketopyrrolopyrrole-Based Polymer: The Impact of a High Dopant Strength and Good Structural Order. *Adv. Mater.* **2016**, *28*, 6003−6010.
(16) Dai, A.; Zhou, Y.; Shu, A. L.; Mohapatra, S. K.; Wang, H.; Fuentes-Hernandez, C.; Zhang, Y.; Barlow, S.; Loo, Y.-L.; Marder, S. R.; Kippelen, B.; Kahn, A. Enhanced Charge-Carrier Injection and Collection Via Lamination of Doped Polymer Layers p-Doped with a Solution-Processible Molybdenum Complex. *Adv. Funct. Mater.* **2014**, *24*, 2197−2204.
(17) Suh, E. H.; Kim, S. B.; Jung, J.; Jang, J. Extremely Electron-Withdrawing Lewis-Paired CN Groups for Organic p-Dopants. *Angew. Chem., Int. Ed.* **2023**, *62*, No. e202304245.
(18) Lin, X.; Wegner, B.; Lee, K. M.; Fusella, M. A.; Zhang, F.; Moudgil, K.; Rand, B. P.; Barlow, S.; Marder, S. R.; Koch, N.; Kahn, A. Beating the thermodynamic limit with photo-activation of n-doping in organic semiconductors. *Nat. Mater.* **2017**, *16*, 1209−1215.
(19) Li, J.; Zhao, Y.; Tan, H. S.; Guo, Y. L.; Di, C. A.; Yu, G.; Liu, Y. Q.; Lin, M.; Lim, S. H.; Zhou, Y. H.; Su, H. B.; Ong, B. S. A stable solution-processed polymer semiconductor with record high-mobility for printed transistors. *Sci. Rep.* **2012**, *2*, No. 754.
(20) Ji, Y.; Xiao, C.; Wang, Q.; Zhang, J.; Li, C.; Wu, Y.; Wei, Z.; Zhan, X.; Hu, W.; Wang, Z.; Janssen, R. A. J.; Li, W. Asymmetric Diketopyrrolopyrrole Conjugated Polymers for Field-Effect Transistors and Polymer Solar Cells Processed from a Nonchlorinated Solvent. *Adv. Mater.* **2016**, *28*, 943−950.
(21) Wang, D.; Ding, J.; Dai, X.; Xiang, L.; Ye, D.; He, Z.; Zhang, F.; Jung, S.-H.; Lee, J.-K.; Di, C.-A.; Zhu, D. Triggering ZT to 0.40 by Engineering Orientation in One Polymeric Semiconductor. *Adv. Mater.* **2023**, *35*, No. 2208215.
(22) Ding, J.; Liu, Z.; Zhao, W.; Jin, W.; Xiang, L.; Wang, Z.; Zeng, Y.; Zou, Y.; Zhang, F.; Yi, Y.; Diao, Y.; McNeill, C. R.; Di, C. A.; Zhang, D.; Zhu, D. Selenium-Substituted Diketopyrrolopyrrole Polymer for High-Performance p-Type Organic Thermoelectric Materials. *Angew. Chem., Int. Ed.* **2019**, *58*, 18994−18999.
(23) Han, J.; Jiang, Y.; Tiernan, E.; Ganley, C.; Song, Y.; Lee, T.; Chiu, A.; McGuiggan, P.; Adams, N.; Clancy, P.; Russell, T. P.; Hopkins, P. E.; Thon, S. M.; Tovar, J. D.; Katz, H. E. Blended Conjugated Host and Unconjugated Dopant Polymers Towards N-type All-Polymer Conductors and High-ZT Thermoelectrics. *Angew. Chem., Int. Ed.* **2023**, *62*, No. e202219313.
(24) Wang, D.; Ding, J.; Ma, Y.; Xu, C.; Li, Z.; Zhang, X.; Zhao, Y.; Zhao, Y.; Di, Y.; Liu, L.; Dai, X.; Zou, Y.; Kim, B.; Zhang, F.; Liu, Z.; McCulloch, I.; Lee, M.; Chang, C.; Yang, X.; Wang, D.; Zhang, D.; Zhao, L.-D.; Di, C.-A.; Zhu, D. Multi-heterojunctioned Plastics with High Thermoelectric Figure-of-merit. *Nature* **2024**, DOI: 10.1038/s41586-024-07724-2. in press.
(25) Di Nuzzo, D.; Fontanesi, C.; Jones, R.; Allard, S.; Dumsch, I.; Scherf, U.; von Hauff, E.; Schumacher, S.; Da Como, E. How intermolecular geometrical disorder affects the molecular doping of donor-acceptor copolymers. *Nat. Commun.* **2015**, *6*, No. 6460.
(26) Zhang, Y.; Blom, P. W. M. Electron and hole transport in poly(fluorene-benzothiadiazole). *Appl. Phys. Lett.* **2011**, *98*, No. 143504.
(27) Li, H.; Song, J.; Xiao, J.; Wu, L.; Katz, H. E.; Chen, L. Synergistically Improved Molecular Doping and Carrier Mobility by Copolymerization of Donor−Acceptor and Donor−Donor Building Blocks for Thermoelectric Application. *Adv. Funct. Mater.* **2020**, *30*, No. 2004378.
(28) Jacobs, I. E.; D'Avino, G.; Lemaur, V.; Lin, Y.; Huang, Y.; Chen, C.; Harrelson, T. F.; Wood, W.; Spalek, L. J.; Mustafa, T.; O'Keefe, C. A.; Ren, X.; Simatos, D.; Tjhe, D.; Statz, M.; Strzalka, J. W.; Lee, J. K.; McCulloch, I.; Fratini, S.; Beljonne, D.; Sirringhaus, H. Structural and Dynamic Disorder, Not Ionic Trapping, Controls Charge Transport in Highly Doped Conducting Polymers. *J. Am. Chem. Soc.* **2022**, *144*, 3005−3019.
(29) Gregory, S. A.; Hanus, R.; Atassi, A.; Rinehart, J. M.; Wooding, J. P.; Menon, A. K.; Losego, M. D.; Snyder, G. J.; Yee, S. K. Quantifying charge carrier localization in chemically doped semiconducting polymers. *Nat. Mater.* **2021**, *20*, 1414−1421.
(30) Zhong, Y.; Untilova, V.; Muller, D.; Guchait, S.; Kiefer, C.; Herrmann, L.; Zimmermann, N.; Brosset, M.; Heiser, T.; Brinkmann, M. Preferential Location of Dopants in the Amorphous Phase of Oriented Regioregular Poly(3-hexylthiophene-2,5-diyl) Films Helps Reach Charge Conductivities of 3000 S $cm^{-1}$. *Adv. Funct. Mater.* **2022**, *32*, No. 2202075.
(31) Yamashita, Y.; Tsurumi, J.; Ohno, M.; Fujimoto, R.; Kumagai, S.; Kurosawa, T.; Okamoto, T.; Takeya, J.; Watanabe, S. Efficient molecular doping of polymeric semiconductors driven by anion exchange. *Nature* **2019**, *572*, 634−638.
(32) Guo, H.; Yang, C. Y.; Zhang, X.; Motta, A.; Feng, K.; Xia, Y.; Shi, Y.; Wu, Z.; Yang, K.; Chen, J.; Liao, Q.; Tang, Y.; Sun, H.; Woo, H. Y.; Fabiano, S.; Facchetti, A.; Guo, X. Transition metal-catalysed molecular n-doping of organic semiconductors. *Nature* **2021**, *599*, 67−73.
(33) Jin, W.; Yang, C.-Y.; Pau, R.; Wang, Q.; Tekelenburg, E. K.; Wu, H.-Y.; Wu, Z.; Jeong, S. Y.; Pitzalis, F.; Liu, T.; He, Q.; Li, Q.; Huang, J.-D.; Kroon, R.; Heeney, M.; Woo, H. Y.; Mura, A.; Motta, A.; Facchetti, A.; Fahlman, M.; Loi, M. A.; Fabiano, S. Photocatalytic doping of organic semiconductors. *Nature* **2024**, *630*, 96−101.
(34) Bauer, A.; Westkämper, F.; Grimme, S.; Bach, T. Catalytic enantioselective reactions driven by photoinduced electron transfer. *Nature* **2005**, *436*, 1139−1140.
(35) Schwarze, M.; Gaul, C.; Scholz, R.; Bussolotti, F.; Hofacker, A.; Schellhammer, K. S.; Nell, B.; Naab, B. D.; Bao, Z.; Spoltore, D.; Vandewal, K.; Widmer, J.; Kera, S.; Ueno, N.; Ortmann, F.; Leo, K. Molecular parameters responsible for thermally activated transport in doped organic semiconductors. *Nat. Mater.* **2019**, *18*, 242−248.
(36) Shao, R.-Y.; Xu, X.-C.; Zhou, Z.-H.; Zeng, W.-J.; Song, T.-W.; Yin, P.; Li, A.; Ma, C.-S.; Tong, L.; Kong, Y.; Liang, H.-W. Promoting ordering degree of intermetallic fuel cell catalysts by low-melting-point metal doping. *Nat. Commun.* **2023**, *14*, No.5896.
(37) Dai, X.; Liu, L.; Ji, Z.; Meng, Q.; Zou, Y. Surface charge transfer doping of graphene using a strong molecular dopant CN6-CP. *Chin. Chem. Lett.* **2023**, *34*, No. 107239.
(38) Zhao, W. R.; Dai, X. J.; Liu, L. Y.; Meng, Q.; Zou, Y.; Di, C. A.; Zhu, D. B. Enhanced thermoelectric performance of pentacene via surface charge transfer doping in a sandwich structure. *Appl. Phys. Lett.* **2021**, *118*, No. 253302.
(39) Mousley, P. J.; Rochford, L. A.; Ryan, P. T. P.; Blowey, P.; Lawrence, J.; Duncan, D. A.; Hussain, H.; Sohail, B.; Lee, T.-L.; Bell, G. R.; Costantini, G.; Maurer, R. J.; Nicklin, C.; Woodruff, D. P. Direct Experimental Evidence for Substrate Adatom Incorporation into a Molecular Overlayer. *J. Phys. Chem. C* **2022**, *126*, 7346−7355.
(40) Wu, S.; Wu, X.; Xing, W.; Sun, Y.; Zou, Y.; Xu, W.; Zhu, D. Backbone Structure Effect on the Thermoelectric Properties of IDT-Based p-Type Conjugated Polymers. *Macromol. Rapid Commun.* **2020**, *41*, No. 1900322.
(41) Zhang, Q.; Sun, Y.; Xu, W.; Zhu, D. Thermoelectric energy from flexible P3HT films doped with a ferric salt of triflimide anions. *Energy Environ. Sci.* **2012**, *5*, 9639−9644.
(42) Yoon, J. W.; Kumar, A.; Kumar, P.; Hippalgaonkar, K.; Senthilnath, J.; Chellappan, V. Explainable machine learning to enable


https://doi.org/10.1021/jacsau.4c00567
*JACS Au* 2024, 4, 3884−3895

high-throughput electrical conductivity optimization and discovery of doped conjugated polymers. *Knowledge-Based Syst.* **2024**, *295*, No. 111812.
(43) Liang, Z.; Choi, H. H.; Luo, X.; Liu, T.; Abtahi, A.; Ramasamy, U. S.; Hitron, J. A.; Baustert, K. N.; Hempel, J. L.; Boehm, A. M.; Ansary, A.; Strachan, D. R.; Mei, J.; Risko, C.; Podzorov, V.; Graham, K. R. n-type charge transport in heavily p-doped polymers. *Nat. Mater.* **2021**, *20*, 518−524.
(44) Scheunemann, D.; Järsvall, E.; Liu, J.; Beretta, D.; Fabiano, S.; Caironi, M.; Kemerink, M.; Müller, C. Charge transport in doped conjugated polymers for organic thermoelectrics. *Chem. Phys. Rev.* **2022**, *3*, No. 021309.
(45) Chen, K.; Hu, H.; Song, I.; Gobeze, H. B.; Lee, W.-J.; Abtahi, A.; Schanze, K. S.; Mei, J. Organic optoelectronic synapse based on photon-modulated electrochemical doping. *Nat. Photonics* **2023**, *17*, 629−637.
(46) Wei, X.; Zhang, P.; Xu, T.; Zhou, H.; Bai, Y.; Chen, Q. Chemical approaches for electronic doping in photovoltaic materials beyond crystalline silicon. *Chem. Soc. Rev.* **2022**, *51*, 10016−10063.
(47) Grancini, G.; Maiuri, M.; Fazzi, D.; Petrozza, A.; Egelhaaf, H. J.; Brida, D.; Cerullo, G.; Lanzani, G. Hot exciton dissociation in polymer solar cells. *Nat. Mater.* **2013**, *12*, 29−33.
(48) Yam, V. W.-W. Using synthesis to steer excited states and their properties and functions. *Nat. Synth.* **2023**, *2*, 94−100.
(49) Frisch, M. J.; Trucks, G. W.; Schlegel, H. B.; Scuseria, G. E.; Robb, M. A.; Cheeseman, J. R.; Scalmani, G.; Barone, V.; Petersson, G. A.; Nakatsuji, H.; Caricato, M.; Li, X.; Hratchian, H. P.; Izmaylov, A. F.; Bloino, J.; Zheng, G.; Sonnenberg, J. L.; Hada, M.; Ehara, M.; Toyota, K.; Fukuda, R.; Hasegawa, J.; Ishida, M.; Nakajima, T.; Honda, Y.; Kitao, O.; Nakai, H.; Vreven, T.; Montgomery, J. A.; Peralta, J. E.; Ogliaro, F.; Bearpark, M.; Heyd, J. J.; Brothers, E. N.; Kudin, K. N.; Staroverov, V. N.; Keith, T.; Kobayashi, R.; Normand, J.; Raghavachari, K.; Rendell, A.; Burant, J. C.; Iyengar, S. S.; Tomasi, J.; Cossi, M.; Rega, N.; Millam, J. M.; Klene, M.; Knox, J. E.; Cross, J. B.; Bakken, V.; Adamo, C.; Jaramillo, J.; Gomperts, R.; Stratmann, R. E.; Yazyev, O.; Austin, A. J.; Cammi, R.; Pomelli, C.; Ochterski, J. W.; Martin, R. L.; Morokuma, K.; Zakrzewski, V. G.; Voth, G. A.; Salvador, P.; Dannenberg, J. J.; Dapprich, S.; Daniels, A. D.; Farkas, O.; Foresman, J. B.; Ortiz, J. V.; Cioslowski, J.; Fox, D. J. *Gaussian 09, revision D.01*; Gaussian Inc.: Wallingford, CT, 2013.
(50) Lu, T.; Chen, F. Multiwfn: A multifunctional wavefunction analyzer. *J. Comput. Chem.* **2012**, *33*, 580−592.
(51) Olthof, S.; Mehraeen, S.; Mohapatra, S. K.; Barlow, S.; Coropceanu, V.; Brédas, J.-L.; Marder, S. R.; Kahn, A. Ultralow Doping in Organic Semiconductors: Evidence of Trap Filling. *Phys. Rev. Lett.* **2012**, *109*, No. 176601.
(52) Ji, Z.; Zhao, W.; Xiang, L.; Ding, J.; Wang, D.; Dai, X.; Liu, L.; Zhang, F.; Zou, Y.; Di, C.-A. Hierarchical Heterojunction Enhanced Photodoping of Polymeric Semiconductor for Photodetection and Photothermoelectric Applications. *ACS Materials Lett.* **2022**, *4*, 815−822.
(53) Zhang, Z.; Xu, C.; Sun, Q.; Zhu, Y.; Yan, W.; Cai, G.; Li, Y.; Si, W.; Lu, X.; Xu, W.; Yang, Y.; Lin, Y. Delocalizing Excitation for Highly-Active Organic Photovoltaic Catalysts. *Angew. Chem., Int. Ed.* **2024**, *63*, No. e202402343.
(54) Roy, P.; Jha, A.; Yasarapudi, V. B.; Ram, T.; Puttaraju, B.; Patil, S.; Dasgupta, J. Ultrafast bridge planarization in donor-$\pi$-acceptor copolymers drives intramolecular charge transfer. *Nat. Commun.* **2017**, *8*, No. 1716.
(55) Wang, K.; Chen, H.; Li, S.; Zhang, J.; Zou, Y.; Yang, Y. Interplay between Intrachain and Interchain Excited States in Donor−Acceptor Copolymers. *J. Phys. Chem. B* **2021**, *125*, 7470−7476.
(56) Guo, Z.; Lee, D.; Schaller, R. D.; Zuo, X.; Lee, B.; Luo, T.; Gao, H.; Huang, L. Relationship between Interchain Interaction, Exciton Delocalization, and Charge Separation in Low-Bandgap Copolymer Blends. *J. Am. Chem. Soc.* **2014**, *136*, 10024−10032.
(57) Falke, S. M.; Rozzi, C. A.; Brida, D.; Maiuri, M.; Amato, M.; Sommer, E.; De Sio, A.; Rubio, A.; Cerullo, G.; Molinari, E.; Lienau, C. Coherent ultrafast charge transfer in an organic photovoltaic blend. *Science* **2014**, *344*, 1001−1005.
(58) Ji, Z.; Li, Z.; Liu, L.; Zou, Y.; Di, C.-A.; Zhu, D. Organic Thermoelectric Devices for Energy Harvesting and Sensing Applications. *Adv. Mater. Technol.* **2024**, No. 2302128.
(59) Gao, C.; Li, C.; Yang, Y.; Jiang, Z.; Xue, X.; Chenchai, K.; Liao, J.; Shangguan, Z.; Wu, C.; Zhang, X.; Jia, D.; Zhang, F.; Liu, G.; Zhang, G.; Zhang, D. Nonhalogenated Solvent Processable and High-Density Photopatternable Polymer Semiconductors Enabled by Incorporating Hydroxyl Groups in the Side Chains. *Adv. Mater.* **2024**, *36*, No. 2309256.
(60) Xie, Y.; Ding, C.; Jin, Q.; Zheng, L.; Xu, Y.; Xiao, H.; Cheng, M.; Zhang, Y.; Yang, G.; Li, M.; Li, L.; Liu, M. Organic transistor-based integrated circuits for future smart life. *SmartMat* **2024**, No. e1261.
(61) Jiang, B.; Han, X.; Che, Y.; Li, W.; Zheng, H.; Li, J.; Ou, C.; Dou, N.; Han, Z.; Ji, T.; Liu, C.; Zhao, Z.; Guo, Y.; Liu, Y.; Zhang, L. Flexible organic integrated circuits free of parasitic capacitance fabricated through a simple dual self-alignment method. *SmartMat* **2024**, No. e1273.
(62) Jie, J.; Liu, Y.; Cong, L.; Zhang, B.; Lu, W.; Zhang, X.; Liu, J.; Xie, H.; Sun, L. High-performance PVDF-HFP based gel polymer electrolyte with a safe solvent in Li metal polymer battery. *J. Energy Chem.* **2020**, *49*, 80−88.
(63) Xiang, L.; He, Z.; Yan, C.; Zhao, Y.; Li, Z.; Jia, L.; Jiang, Z.; Dai, X.; Lemaur, V.; Ma, Y.; Liu, L.; Meng, Q.; Zou, Y.; Beljonne, D.; Zhang, F.; Zhang, D.; Di, C.-A.; Zhu, D. Nanoscale doping of polymeric semiconductors with confined electrochemical ion implantation. *Nat. Nanotechnol.* **2024**, DOI: 10.1038/s41565-024-01653-x. in press.
(64) Ke, Z.; Ahmed, M. H.; Abtahi, A.; Hsu, S.-H.; Wu, W.; Espenship, M. F.; Baustert, K. N.; Graham, K. R.; Laskin, J.; Pan, L.; Mei, J. Thermally Activated Aromatic Ionic Dopants (TA-AIDs) Enabling Stable Doping, Orthogonal Processing and Direct Patterning. *Adv. Funct. Mater.* **2023**, *33*, No. 2211522.
(65) Perevedentsev, A.; Campoy-Quiles, M. Rapid and high-resolution patterning of microstructure and composition in organic semiconductors using 'molecular gates'. *Nat. Commun.* **2020**, *11*, No. 3610.
(66) Bubnova, O.; Crispin, X. Towards polymer-based organic thermoelectric generators. *Energy Environ. Sci.* **2012**, *5*, 9345−9362.
(67) Linseis, V.; Völklein, F.; Reith, H.; Nielsch, K.; Woias, P. Advanced platform for the in-plane ZT measurement of thin films. *Rev. Sci. Instrum.* **2018**, *89*, No. 015110.
(68) Ke, Z.; Abtahi, A.; Hwang, J.; Chen, K.; Chaudhary, J.; Song, I.; Perera, K.; You, L.; Baustert, K. N.; Graham, K. R.; Mei, J. Highly Conductive and Solution-Processable n-Doped Transparent Organic Conductor. *J. Am. Chem. Soc.* **2023**, *145*, 3706−3715.
(69) Tang, H.; Liang, Y.; Liu, C.; Hu, Z.; Deng, Y.; Guo, H.; Yu, Z.; Song, A.; Zhao, H.; Zhao, D.; Zhang, Y.; Guo, X.; Pei, J.; Ma, Y.; Cao, Y.; Huang, F. A solution-processed n-type conducting polymer with ultrahigh conductivity. *Nature* **2022**, *611*, 271−277.


https://doi.org/10.1021/jacsau.4c00567
*JACS Au* 2024, 4, 3884−3895